A R C H I V E O F M E C H A N I C A L E N G I N E E R I N G

VOL. LXV 2018 Number 3

DOI: 10.24425/124491

**Key words:** tubular joint, adhesive, composite, adherend, peel, shear stress

*EHSAN SELAHI*[1]

# ELASTICITY SOLUTION OF ADHESIVE TUBULAR JOINTS IN LAMINATED COMPOSITES WITH AXIAL SYMMETRY

This paper presents an elasticity solution of adhesive tubular joints in laminated composites, with axial symmetry. In this model, adherends are orthotropic shells and the stacking sequences can be either symmetric or asymmetric. Adhesive layer is homogenous and made of isotropic material. They are modelled as continuously distributed tension/compression and shear springs. Employing constitutive, kinematics and equilibrium equations, sets of differential equations for each inside and outside of overlap zones are obtained. By solving these equations, shear and peel stresses in adhesive layer(s), as well as deflections, stress resultants and moment resultants in the adherends are determined. It is seen that the magnitude of peel stresses due to transverse shear stress resultant is much greater than that obtained from axial stress resultant. The developed results are compared with those obtained by finite element analysis using ANSYS software. The comparisons demonstrate the accuracy and effectiveness of the aforementioned methods.

## 1. Introduction

The history of using composite materials in piping systems is close to half a century. Several advantages of composite pipes with respect to metallic pipes such as: light weight, high specific strength and stiffness and corrosion resistance, caused widespread tendency to using of these pipes in various industries such as: oil, gas, petrochemical, power plants, marine industries and sewage pipes.

Joints are the source of weakness and structural excess weight. Therefore, the ideal piping system would be designed without joints. However, limitations on component size imposed by manufacturing process and transportation necessitate applying joints in most piping systems. Adhesive joint is a simple method with

[1] *Department of Mechanical Engineering, Marvdasht Branch, Islamic Azad University, Marvdasht, Iran, Post code 73711-13119. Email: selahi@miau.ac.ir*

low weight and cost for joining composite pipes together. Advantages of adhesive joints with respect to mechanical joints (screws and rivets) are:

- significant reduction in stress concentration,
- weight reduction (especially in narrow joints),
- vibration damping capability,
- capability of joining and sealing simultaneously,
- ease of fabrication process,
- reducing production cost.

The most common type of pipe joint is the tubular lap joint. The other common types of pipe joints are: tubular butt and tubular strap joints. These joints are shown in Fig. 1).

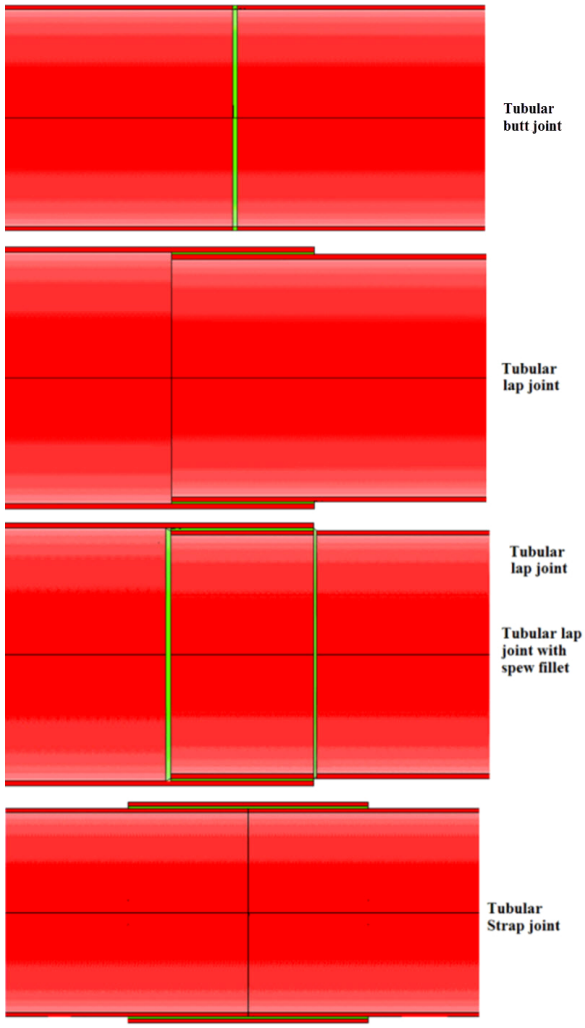


Fig. 1. Typical tubular adhesive joint

The response of an adhesive annular butt joint subjected to a pure torsion was measured in [1]. Authors of [2], analysed the stresses in tubular lap joints under a tensile axial load and gave solutions for both the shear stress $\tau_{zr}$ in the adhesive layer and normal stress $\sigma_r$ across the thickness of the adhesive layer that result from adherend bending.

The problem of torsional stress in tubular lap joints was first investigated in [3]. In this analysis, the presence of the circumferential shear stress was ignored, and the adhesive layer was treated as a sort of shearing springs acting between two adherends. The previous research was improved by taking into account the effect of thickness of the adhesive layer [4]. Stress distribution formulation for adhesively bonded tubular lap joint under torsion was carried out in [5]. This research is based on the variational principle of complementary energy method.

All the above models considered only the isotropic adherends. Authors of [6], applied finite element method for analysis of the tubular lap joint composed of steel tube that adhesively bonded to a composite tube. The system responses of composite pipe joints with orthotropic behaviour and under tensile loading was investigated in [7, 8] by using one-dimensional simulation model.

Behaviour of GFRP adhesive pipe joints subjected to pressure and axial loadings was studied experimentally and analytically in [9]. The torsional strength of tubular adhesive joints with carbon-epoxy and glass-epoxy adherends are investigated in [10]. Recently, a closed form solution for tubular adhesive joints subjected to axial loads was presented in [11, 12].

In this paper, we present an analytical model for analysing of adhesive joints in laminated composite pipes with axial symmetry in the cylindrical coordinates. A sample of tubular lap joint is solved analytically and the results are validated by finite element modelling in ANSYS software.

## 2. Mathematical modelling

### 2.1. Tubular butt joint

In the tubular butt joint, magnitude of peel stress is determined by a simple equation of $\sigma = N_z/t$. In this equation $N_z$ is axial stress resultant and $t$ is thickness of the pipe. The adhesive shear stress is considered to be zero.

### 2.2. Mathematical modelling for other types of tubular adhesive joints

Mathematical modelling for other types of tubular adhesive joints is obtained by adopting sets of restrictive assumptions, for describing the behaviour of bonded joints. Based on these assumptions, constitutive and kinematics relations for each of adherends and constitutive relations for adhesive layer are obtained. Then, equilibrium equations of the joint in each of inside and outside of overlap zones are derived. Finally, by combining these relations and equations, governing equations

as sets of differential equations, for each zone (inside and outside of overlap zone) are obtained. Basic assumptions for the adherends, adhesive layers, loading and boundary conditions are as follows:

1. Adherends
   - adherends are modelled as axisymmetric, laminated composite pipes;
   - the thickness of layers remains constant;
   - laminates have linear elastic behaviour.
2. Adhesive layers
   - adhesive layer is assumed to behave as homogenous, isotropic and elastic material and modelled as continuously distributed tension compression and shear springs.

As noted, each type of adhesive joint consists of two regions of: inside of overlap zone and outside of overlap zone, and the governing equations in these two regions are different. It is clear that this equation in the inside of overlap zone is more complex than the governing equations in outside of overlap zones.

### 2.3. Inside of overlap zone modelling

As mentioned previously, the adherends are assumed to have linear elastic behaviour and the thickness of adherends remain constant when subjected to loadings. Therefore, the displacements and slopes in the cylindrical coordinates are defined as:

$$u_r^i = u_r^i(z), \tag{1}$$

$$u_\theta^i(z) = u_{\theta 0}^i(z) - \xi\, \beta_\theta^i(z), \tag{2}$$

$$u_z^i(z) = u_{z0}^i(z) - \xi\, \beta_z^i(z), \tag{3}$$

$$\beta_\theta^i = \frac{\partial u_r^i}{\partial \theta} = 0, \tag{4}$$

$$\beta_z^i = \frac{\partial u_r^i}{\partial z}, \tag{5}$$

where $\xi = r - \overline{r}$ and $\overline{r}$ is the mean radius of the tubular adherend. The strain–displacement relations for axisymmetric cylindrical shells become:

$$\varepsilon_{\theta\theta} = \frac{u_r(z)}{r}, \tag{6}$$

$$\varepsilon_{zz} = \frac{\partial u_z}{\partial z}, \tag{7}$$

$$\gamma_{z\theta} = \frac{\partial u_\theta}{\partial z}. \tag{8}$$

By considering $r \gg t$, the tangential strain remains constant in the radial direction and is equal to:

$$\varepsilon^0_{\theta\theta} = \frac{u_r(z)}{\bar{r}}\,. \tag{9}$$

The resultant force (moment)–strain relations for cylindrical coordinate in the $\theta$–$z$ plane are defined as:

$$\begin{bmatrix} N_Z \\ N_\theta \\ N_{Z\theta} \end{bmatrix} = \begin{bmatrix} A_{11} & A_{12} & A_{16} \\ A_{12} & A_{22} & A_{26} \\ A_{16} & A_{26} & A_{66} \end{bmatrix} \begin{bmatrix} \varepsilon^0_z \\ \varepsilon^0_\theta \\ \gamma^0_{z\theta} \end{bmatrix} + \begin{bmatrix} B_{11} & B_{12} & B_{16} \\ B_{12} & B_{22} & B_{26} \\ B_{16} & B_{26} & B_{66} \end{bmatrix} \begin{bmatrix} \kappa_z \\ \kappa_\theta \\ \kappa_{z\theta} \end{bmatrix}, \tag{10}$$

$$\begin{bmatrix} M_z \\ M_\theta \\ M_{z\theta} \end{bmatrix} = \begin{bmatrix} B_{11} & B_{12} & B_{16} \\ B_{12} & B_{22} & B_{26} \\ B_{16} & B_{26} & B_{66} \end{bmatrix} \begin{bmatrix} \varepsilon^0_z \\ \varepsilon^0_\theta \\ \gamma^0_{z\theta} \end{bmatrix} + \begin{bmatrix} D_{11} & D_{12} & B_{16} \\ D_{12} & D_{22} & D_{26} \\ D_{16} & D_{26} & D_{66} \end{bmatrix} \begin{bmatrix} \kappa_z \\ \kappa_\theta \\ \kappa_{z\theta} \end{bmatrix}, \tag{11}$$

where:

$$\begin{bmatrix} \kappa_z \\ \kappa_\theta \\ \kappa_{z\theta} \end{bmatrix} = - \begin{bmatrix} \dfrac{\partial^2 u_r}{\partial z^2} \\ \dfrac{\partial^2 u_r}{\partial \theta^2} \\ 2\dfrac{\partial^2 u_r}{\partial z \partial \theta} \end{bmatrix} = \begin{bmatrix} -\dfrac{\partial^2 u_r}{\partial z^2} \\ 0 \\ 0 \end{bmatrix} \tag{12}$$

and $\boldsymbol{A}$, $\boldsymbol{B}$ and $\boldsymbol{D}$ are extensional, coupling and bending stiffness matrices, respectively, and defined by Eqs. (13)–(15):

$$A_{ij} = \sum_{k=1}^{n} (\overline{Q}_{ij})_k (z_k - z_{k-1}), \tag{13}$$

$$B_{ij} = \frac{1}{2} \sum_{k=1}^{n} (\overline{Q}_{ij})_k (z_k^2 - z_{k-1}^2), \tag{14}$$

$$D_{ij} = \frac{1}{3} \sum_{k=1}^{n} (\overline{Q}_{ij})_k (z_k^3 - z_{k-1}^3), \tag{15}$$

where $\boldsymbol{Q}$ denotes the stiffness matrix [13]. By substituting Eqs. (1)–(8) into Eqs. (10) and (11), the resultants force and moment equations are obtained as:

$$N_z = A_{11}\frac{\partial u_{z0}}{\partial z} + A_{12}\frac{u_r}{\bar{r}} + A_{16}\frac{\partial u_\theta}{\partial z} - B_{11}\frac{\partial \beta_z}{\partial z}\,, \tag{16}$$

$$N_\theta = A_{21}\frac{\partial u_{z0}}{\partial z} + A_{22}\frac{u_r}{\bar{r}} + A_{26}\frac{\partial u_\theta}{\partial z} - B_{21}\frac{\partial \beta_z}{\partial z}\,, \tag{17}$$

$$N_{z\theta} = A_{61}\frac{\partial u_{z0}}{\partial z} + A_{62}\frac{u_r}{\bar{r}} + A_{66}\frac{\partial u_\theta}{\partial z} - B_{61}\frac{\partial \beta_z}{\partial z}\,, \tag{18}$$

$$M_z = B_{11}\frac{\partial u_{z0}}{\partial z} + B_{12}\frac{u_r}{\bar{r}} + B_{16}\frac{\partial u_\theta}{\partial z} - D_{11}\frac{\partial \beta_z}{\partial z}, \tag{19}$$

$$M_\theta = B_{21}\frac{\partial u_{z0}}{\partial z} + B_{22}\frac{u_r}{\bar{r}} + B_{26}\frac{\partial u_\theta}{\partial z} - D_{21}\frac{\partial \beta_z}{\partial z}, \tag{20}$$

$$M_{z\theta} = B_{61}\frac{\partial u_{z0}}{\partial z} + B_{62}\frac{u_r}{\bar{r}} + B_{66}\frac{\partial u_\theta}{\partial z} - D_{61}\frac{\partial \beta_z}{\partial z}. \tag{21}$$

By considering the symmetric stacking sequences for adherends, the upper equations are simplified as:

$$\frac{\partial u_{z0}}{\partial z} = \frac{1}{A_{11}}N_z - \frac{A_{12}}{\bar{r}A_{11}}u_r, \tag{22}$$

$$\frac{\partial N_\theta}{\partial z} = \frac{A_{21}}{A_{11}}\frac{\partial N_z}{\partial z} + \left(\frac{A_{22}}{\bar{r}} - \frac{A_{12}^2}{\bar{r}A_{11}}\right)\frac{\partial u_r}{\partial z}, \tag{23}$$

$$\frac{\partial \beta_z}{\partial z} = \frac{-1}{D_{11}}M_z, \tag{24}$$

$$\frac{\partial M_\theta}{\partial z} = \frac{D_{21}}{D_{11}}\frac{\partial M_z}{\partial z}, \tag{25}$$

$$M_{z\theta} = 0. \tag{26}$$

Here, the adhesive layer(s) modelled as continuously distributed linear tension compression and shear springs. In this modelling, shear and peel stresses in the adhesive layer(s) are determined by Eqs. (27) and (28):

$$\sigma(z) = E_a\varepsilon_r(z) = \frac{E_a}{t_a}\left[u_r^i(z) - u_r^j(z)\right], \tag{27}$$

$$\begin{aligned}\tau(z) &= \frac{G_a}{t_a}\left[u_z^i(z,r) - u_z^j(z,r)\right] \\ &= \frac{G_a}{t_a}\left[u_{z0}^i(z) + \frac{t_i}{2}\beta_z^i(z) - u_{z0}^j(z) + \frac{t_j}{2}\beta_z^j(z)\right].\end{aligned} \tag{28}$$

Each equilibrium element in the inside of overlap zone consists of an element of adherend with half thickness of adhesive layer(s). Fig. 2 shows equilibrium elements of tubular lap joint in the inside of overlap zone. The equilibrium equations in the inside of overlap zones in the upper element (Eq. 29) and in the lower element (Eq. 30) are obtained as follows:

$$
\begin{aligned}
\frac{\partial N_z^1}{\partial z} &= -\tau \frac{\left(\bar{r}_1 - \dfrac{t_1 + t_a}{2}\right)}{\bar{r}_1}, \\
\frac{\partial Q_z^1}{\partial z} &= -\frac{N_\theta^1}{\bar{r}_1} - \sigma \frac{\left(\bar{r}_1 - \dfrac{t_1 + t_a}{2}\right)}{\bar{r}_1}, \\
\frac{\partial N_{z\theta}^1}{\partial z} &= 0, \\
\frac{\partial M_{z\theta}^1}{\partial z} &= 0, \\
\frac{\partial M_z^1}{\partial z} &= Q_z^1 - \tau \frac{t_1 + t_a}{2} \frac{\left(\bar{r}_1 - \dfrac{t_1 + t_a}{2}\right)}{\bar{r}_1};
\end{aligned}
\tag{29}
$$

$$
\begin{aligned}
\frac{\partial N_z^2}{\partial z} &= \tau \frac{\left(\bar{r}_2 - \dfrac{t_2 + t_a}{2}\right)}{\bar{r}_2}, \\
\frac{\partial Q_z^2}{\partial z} &= -\frac{N_\theta^2}{\bar{r}_2} + \sigma \frac{\left(\bar{r}_2 - \dfrac{t_2 + t_a}{2}\right)}{\bar{r}_2}, \\
\frac{\partial N_{z\theta}^2}{\partial z} &= 0, \\
\frac{\partial M_{z\theta}^2}{\partial z} &= 0, \\
\frac{\partial M_z^2}{\partial z} &= Q_z^2 - \tau \frac{t_2 + t_a}{2} \frac{\left(\bar{r}_2 - \dfrac{t_2 + t_a}{2}\right)}{\bar{r}_2}.
\end{aligned}
\tag{30}
$$

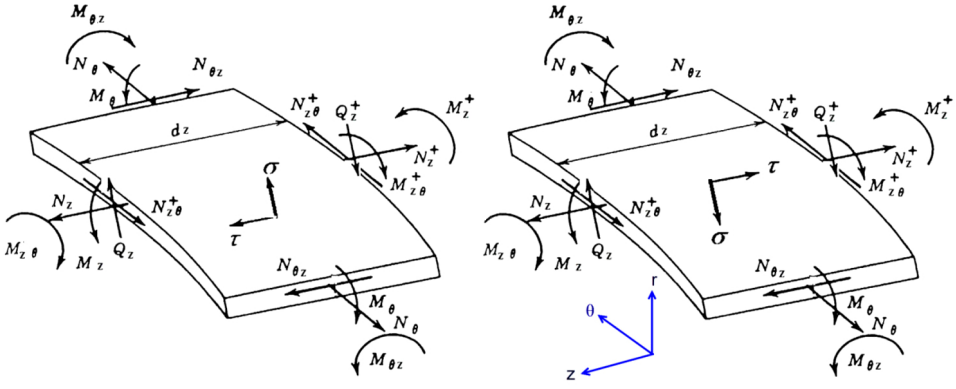


(a) upper adherend (b) lower adherend

Fig. 2. Equilibrium element in the inside of overlap zone

By combining constitutive and kinematic relations of adherends and adhesive layer with equilibrium equations, the governing equations in the inside of overlap zones are determined as sets of coupled differential equations in the form of: $\frac{\mathrm{d}}{\mathrm{d}z}\{X(z)\} = [A]\{X(z)\}$. It has 22 equations and 22 unknowns. Here, for the sake of brevity, only tubular lap adhesive joint governing equation with symmetric stacking sequences is presented as Eq. (A.1) in the appendix section.

### 2.4. Outside of overlap zone modelling

In the outside of overlap zone, constitutive and kinematics relations in adherends are the same as those in the inside of overlap zone. The adhesive stresses don't appear, either. In Fig. 3, an equilibrium element in the outside of overlap zone is shown. So that, the equilibrium equations in the outside of overlap zone are as follows:

$$\begin{aligned}
\frac{\partial N_z^i}{\partial z} &= 0,\\
\frac{\partial Q_z^i}{\partial z} &= -\frac{N_\theta^i}{\bar{r}_i},\\
\frac{\partial N_{z\theta}^i}{\partial z} &= 0,\\
\frac{\partial M_{z\theta}^i}{\partial z} &= 0,\\
\frac{\partial M_z^i}{\partial z} &= Q_z^i.
\end{aligned} \tag{31}$$

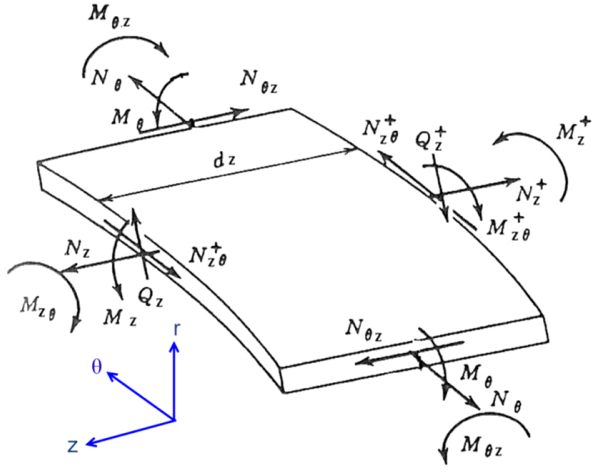


Fig. 3. Equilibrium element in the outside of overlap zones

The governing equations in the outside of overlap zones are sets of differential equations in the form of: $\frac{\mathrm{d}}{\mathrm{d}z}\{X(z)\} = [A]\{X(z)\}$ with 11 equations and 11 unknown as Eq. (32):

$$\begin{cases} \dfrac{\partial u^i_{z0}}{\partial z} = \dfrac{1}{A^i_{11}} N^i_z - \dfrac{A^i_{12}}{\bar{r}_i A^i_{11}} u^i_r, \\ \dfrac{\partial u^i_\theta}{\partial z} = \dfrac{1}{A^i_{66}} N^i_{z\theta}, \\ \dfrac{\partial u^i_r}{\partial z} = \beta^i_z, \\ \dfrac{\partial \beta^i_z}{\partial z} = \dfrac{-1}{D^i_{11}} M^i_z, \\ \dfrac{\partial N^i_z}{\partial z} = 0, \\ \dfrac{\partial N^i_\theta}{\partial z} = \left( \dfrac{A^i_{22}}{\bar{r}_i} - \dfrac{A^{i2}_{12}}{\bar{r}_i A^i_{11}} \right) \beta^i_z, \\ \dfrac{\partial N^i_{z\theta}}{\partial z} = 0, \\ \dfrac{\partial Q^i_z}{\partial z} = -\dfrac{N^i_\theta}{\bar{r}_i}, \\ \dfrac{\partial M^i_z}{\partial z} = Q^i_z, \\ \dfrac{\partial M^i_\theta}{\partial z} = \dfrac{D^i_{21}}{D^i_{11}} Q^i_z, \\ \dfrac{\partial M^i_{z\theta}}{\partial z} = 0. \end{cases} \tag{32}$$

## 3. Numerical results

In this section, an example of adhesive tubular joint with fixed boundary condition in one side and free in the other side is considered. The laminated pipes are manufactured with 8 unidirectional glass/epoxy lamina with the stacking sequences of $[0^\circ, 45^\circ, -45^\circ, 90^\circ]_{Sym}$. The thickness of each lamina is 0.2 mm. The adhesive is Epoxy AY103 (Ciba Geigy). The mechanical properties of adherends and adhesive layer are listed in Table 1. It is noticeable that the symbols $X$, $Y$ and $S$ denote longitudinal tensile strength, transverse tensile strength and in-plane shear strength, respectively.

Table 1.

Mechanical properties of adherends and adhesive layer

| Part | Material | Properties |
|---|---|---|
| Adherend | Fiberglass/Epoxy: | $E_1 = 36.8$ GPa, $E_2 = E_3 = 8.27$ GPa, $G_{12} = G_{13} = 4.14$ GPa, $G_{23} = 3$ GPa, $\nu_{12} = \nu_{13} = 0.26$, $\nu_{23} = 0.38$, $X = 450$ MPa, $Y = 31$ MPa, $S = 72$ MPa, $t = 0.2$ mm |
| Adhesive | Epoxy AY103 (Ciba Geigy) | $E_a = 2.8$ GPa, $\nu_a = 0.4$, $t_a = 0.4$ mm |

The length of each pipe is 70 mm with overlap bonded length of 20 mm. The inner pipe has a mean radius of 25 mm and the outer pipe has a mean radius of 26 mm. The free end of joint is subjected to axial stress resultant of: $N_z$ =10000 N/m and shear stress resultant of $Q_z$ =10 N/m, as shown in Fig. 4.

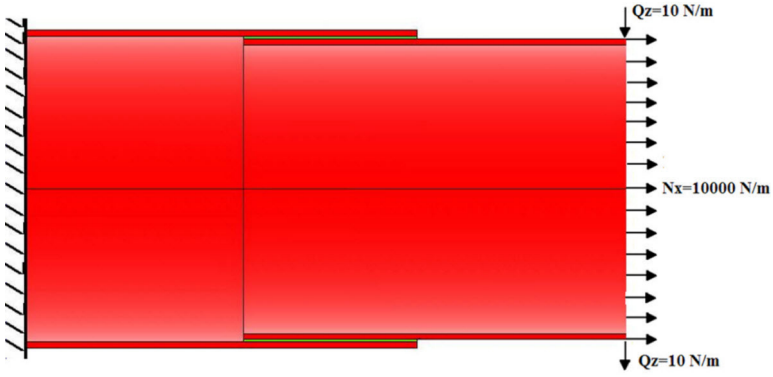


Fig. 4. Boundary conditions and loading

At first, the governing equations in the left outside of overlap zone are solved by using Eq. (32) and by considering the boundary conditions in: $x = -50$ mm. Then, the governing equations in the inside of overlap zone are solved by using equation set A.1. This equation set has an analytical solution in the form of Eq. (33)

$$X = (e^{Ax})X_0 \tag{33}$$

where, $X_0 = X(z = 0)$. Finally, the governing equations in the right outside of overlap zone are solved by using equation set 33 and by considering the boundary conditions in: $x = 20$ mm. Figs. 5 to 8 illustrate deflections, slopes, stress resultants and moment resultants of outer and inner adherends at each point of inside and outside of overlap zones.

Due to the lack of similar solution concerning the problem under consideration in the available literature, the present formulation and method of solu-

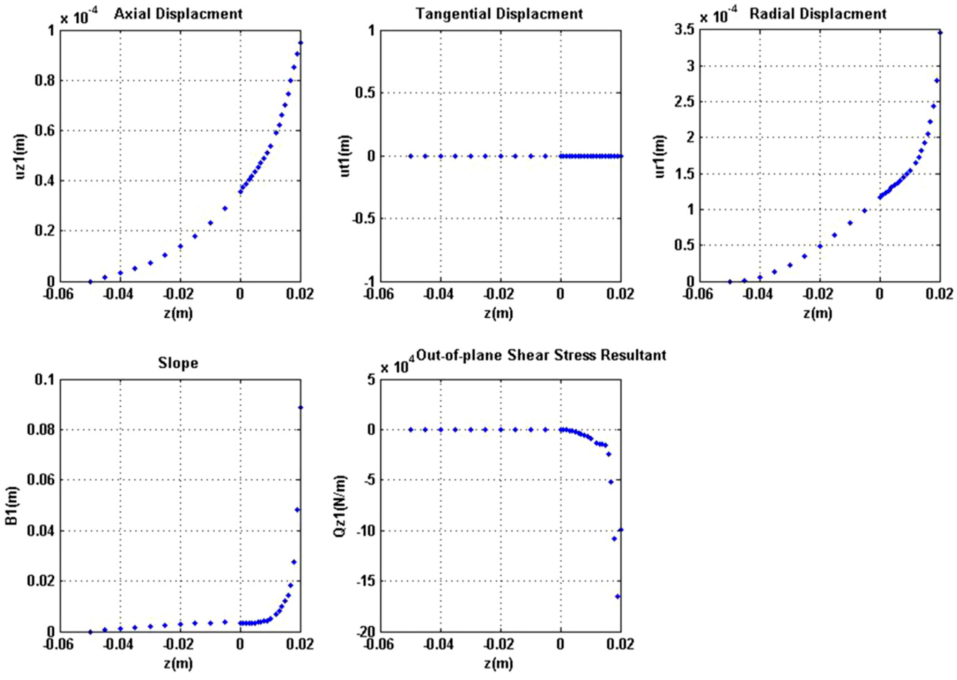


Fig. 5. Deflections and slopes of the outer adherend vs. axial position

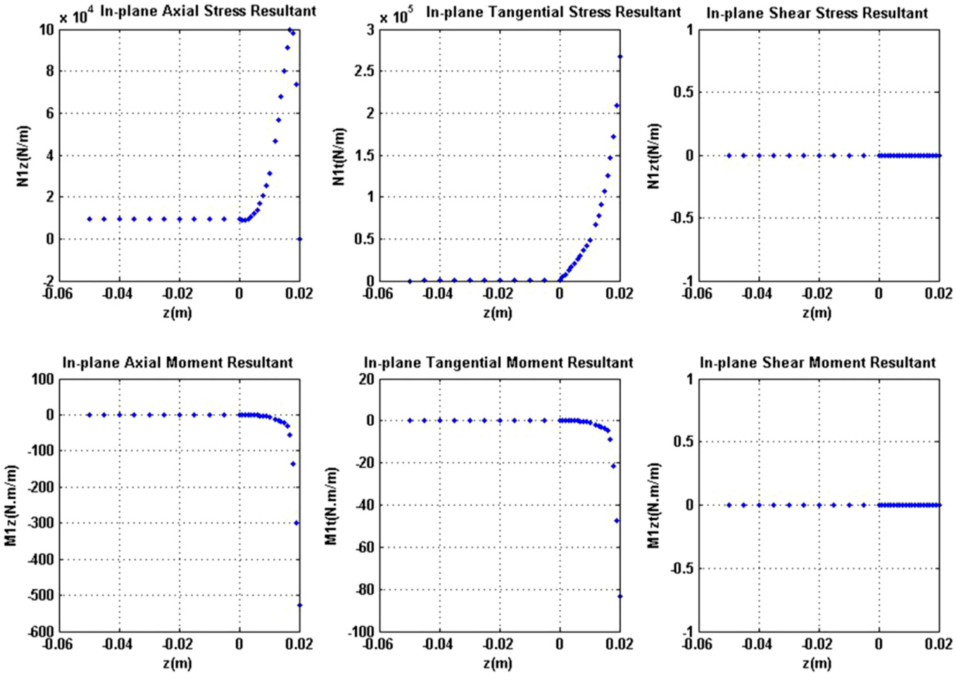


Fig. 6. Stress resultants and moment resultants of the outer adherend vs. axial position

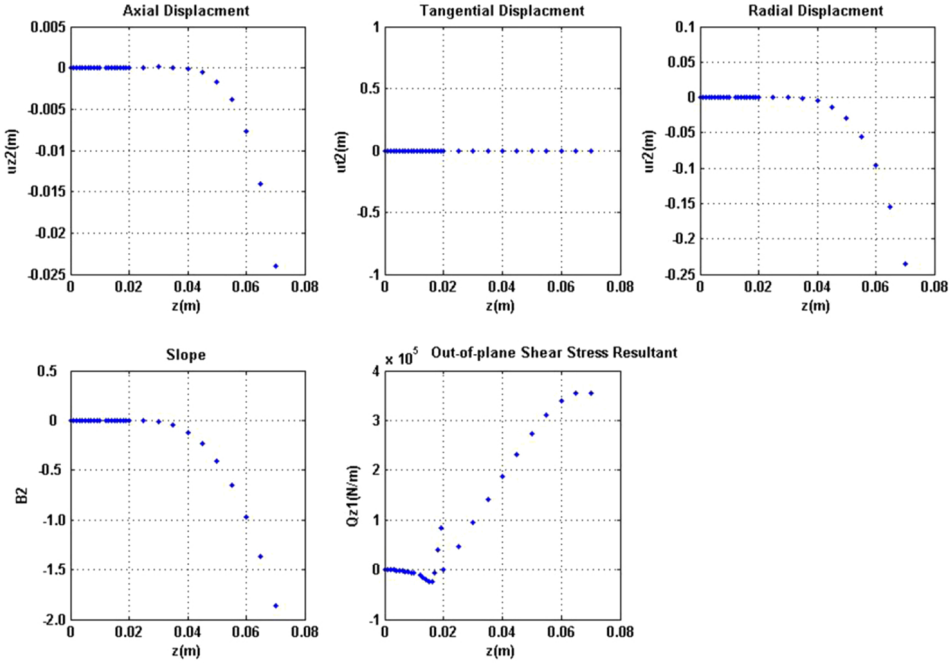


Fig. 7. Deflections and slopes of the inner adherend vs. axial position

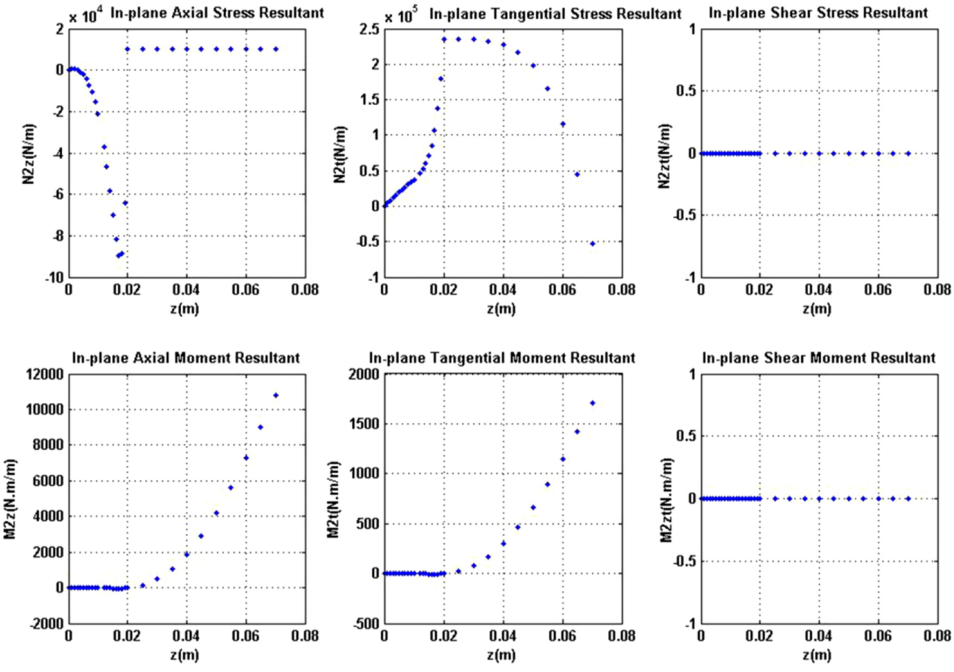


Fig. 8. Stress resultants and moment resultants of the inner adherend vs. axial position

tion are validated by similar modelling obtained by finite element (FE) analysis using ANSYS software. The tubular adhesive joint is modelled by employing 6060, 3D solid elements. Each element consists of 8 nodes. Fig. 9, depicts the variation of peel and shear stresses along the length of overlap zone in the adhesive layer, and the results are compared with those obtained in ANSYS software.

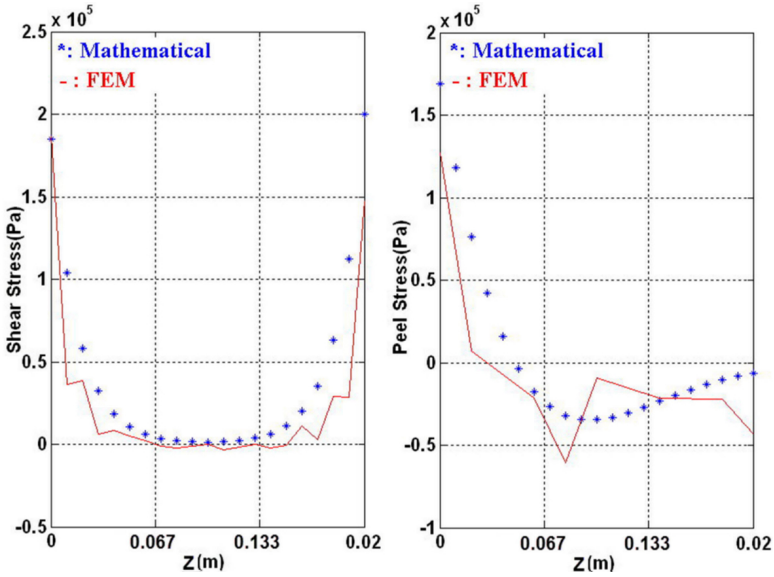


Fig. 9. Peel and shear stress distributions in the adhesive layer

According to Figs. 4 and 9, it is observed that peel stresses, in the adhesive tubular joint, are caused by shear stress resultant of $Q_z$, and the axial stress resultant of $N_z$ has no effect on creation of this type of stress. Although the magnitude of shear stress $Q_z$ resultant is much lower than the magnitude of axial stress resultant $N_z$, the maximum magnitudes of adhesive peel stress is approximately equal to the maximum adhesive shear stress, and this is due to considerable bending moment created by $Q_z$.

It is seen that the maximum magnitudes of peel and shear stresses occur at one edge of overlap zone which is near to the fixed boundary condition. Because of the free surface at the end of the adhesive layer, the adhesive shear stress must be zero. Also, high shear and peel stresses gradient near the end of the joint are observed at a very short distance.

By comparing peel and shear stresses obtained from mathematical modelling and FE simulation, it is seen that the mathematical solutions shows a very good agreement with the results achieved from FE modelling that demonstrates the validity of the presented mathematical modelling.

## 4. Conclusions

In this paper, an efficient analytical elasticity solution of adhesive tubular joints is presented. Here, the adherends are orthotropic shells with linear elastic behaviour. The stacking sequences can be either symmetric or asymmetric. The adhesive layer is considered to be homogenous and made of isotropic material and modelled as continuously distributed tension/compression and shear springs. Finally, by employing constitutive, kinematics and equilibrium equations, sets of differential equations for each inside and outside of overlap zones are derived.

It is found that the presented elasticity solution yields accurate results when compared with the solutions of ANSYS software. The obtained results of the present method reveal the following conclusions:

1. The magnitude of peel stress due to transverse shear resultants is much greater than that obtained from axial stress resultant.
2. The maximum magnitudes of peel and shear stresses occur at one edge of overlap zone which is near to fixed boundary condition.

## Appendix

In the appendix section, the governing equations in the inside of overlap zones for tubular lap adhesive joint with symmetric stacking sequences are presented as Eq. (A.1).

$$
\begin{cases}
\dfrac{\partial u^1_{z0}}{\partial z} = \dfrac{1}{A^1_{11}} N^1_z - \dfrac{A^1_{12}}{\bar{r}_1 A^1_{11}} u^1_r, \\
\dfrac{\partial u^1_{\theta}}{\partial z} = \dfrac{1}{A^1_{66}} N^1_{z\theta}, \\
\dfrac{\partial u^1_{r}}{\partial z} = \beta^1_z, \\
\dfrac{\partial \beta^1_z}{\partial z} = \dfrac{-1}{D^1_{11}} M^1_z, \\
\dfrac{\partial N^1_z}{\partial z} = -\dfrac{\left(\bar{r}_1 - \dfrac{t_1 + t_a}{2}\right)}{\bar{r}_1} \dfrac{G_a}{t_a} \left[ u^2_{z0} + \dfrac{t_2}{2}\beta^2_z - u^1_{z0} + \dfrac{t_1}{2}\beta^1_z \right], \\
\dfrac{\partial N^1_{\theta}}{\partial z} = \dfrac{-A^1_{21}}{A^1_{11}} \dfrac{\left(\bar{r}_1 - \dfrac{t_1 + t_a}{2}\right)}{\bar{r}_1} \dfrac{G_a}{t_a} \left[ u^2_{z0} + \dfrac{t_2}{2}\beta^2_z - u^1_{z0} + \dfrac{t_1}{2}\beta^1_z \right] + \left( \dfrac{A^1_{22}}{\bar{r}_1} - \dfrac{A^{1\,2}_{12}}{\bar{r}_1 A^1_{11}} \right) \beta^1_z,
\end{cases}
$$

$$
\begin{cases}
\dfrac{\partial N^1_{z\theta}}{\partial z} = 0, \\
\dfrac{\partial Q^1_z}{\partial z} = -\dfrac{N^1_\theta}{\bar{r}_1} - \dfrac{\left(\bar{r}_1 - \dfrac{t_1+t_a}{2}\right)}{\bar{r}_1}\dfrac{E_a}{t_a}\left[u^2_r - u^1_r\right], \\
\dfrac{\partial M^1_z}{\partial z} = Q^1_z - \dfrac{t_1+t_a}{2}\dfrac{\left(\bar{r}_1 - \dfrac{t_1+t_a}{2}\right)}{\bar{r}_1}\dfrac{G_a}{t_a}\left[u^2_{z0} + \dfrac{t_2}{2}\beta^2_z - u^1_{z0} + \dfrac{t_1}{2}\beta^1_z\right], \\
\dfrac{\partial M^1_\theta}{\partial z} = \dfrac{D^1_{21}}{D^1_{11}}\left[Q^1_z - \dfrac{t_1+t_a}{2}\dfrac{\left(\bar{r}_1 - \dfrac{t_1+t_a}{2}\right)}{\bar{r}_1}\dfrac{G_a}{t_a}\left[u^2_{z0} + \dfrac{t_2}{2}\beta^2_z - u^1_{z0} + \dfrac{t_1}{2}\beta^1_z\right]\right], \\
\dfrac{\partial M^1_{z\theta}}{\partial z} = 0, \\
\dfrac{\partial u^2_{z0}}{\partial z} = \dfrac{1}{A^2_{11}}N^2_z - \dfrac{A^2_{12}}{\bar{r}_2 A^2_{11}}u^2_r, \\
\dfrac{\partial u^2_\theta}{\partial z} = \dfrac{1}{A^2_{66}}N^2_{z\theta}, \\
\dfrac{\partial u^2_r}{\partial z} = \beta^2_z, \\
\dfrac{\partial \beta^2_z}{\partial z} = \dfrac{-1}{D^2_{11}}M^2_z, \\
\dfrac{\partial N^2_z}{\partial z} = \tau\dfrac{\left(\bar{r}_2 - \dfrac{t_2+t_a}{2}\right)}{\bar{r}_2} = \dfrac{\left(\bar{r}_2 - \dfrac{t_2+t_a}{2}\right)}{\bar{r}_2}\dfrac{G_a}{t_a}\left[u^2_{z0} + \dfrac{t_2}{2}\beta^2_z - u^1_{z0} + \dfrac{t_1}{2}\beta^1_z\right], \\
\dfrac{\partial N^2_\theta}{\partial z} = \dfrac{A^2_{21}}{A^2_{11}}\dfrac{\left(\bar{r}_2 - \dfrac{t_2+t_a}{2}\right)}{\bar{r}_2}\dfrac{G_a}{t_a}\left[u^2_{z0} + \dfrac{t_2}{2}\beta^2_z - u^1_{z0} + \dfrac{t_1}{2}\beta^1_z\right] + \left(\dfrac{A^2_{22}}{\bar{r}_2} - \dfrac{A^{2\,2}_{12}}{\bar{r}_2 A^2_{11}}\right)\beta^2_z, \\
\dfrac{\partial N^2_{z\theta}}{\partial z} = 0, \\
\dfrac{\partial Q^2_z}{\partial z} = -\dfrac{N^2_\theta}{\bar{r}_2} + \dfrac{\left(\bar{r}_2 - \dfrac{t_2+t_a}{2}\right)}{\bar{r}_2}\dfrac{E_a}{t_a}\left[u^2_r - u^1_r\right], \\
\dfrac{\partial M^2_z}{\partial z} = Q^2_z - \dfrac{t_2+t_a}{2}\dfrac{\left(\bar{r}_2 - \dfrac{t_2+t_a}{2}\right)}{\bar{r}_2}\dfrac{G_a}{t_a}\left[u^2_{z0} + \dfrac{t_2}{2}\beta^2_z - u^1_{z0} + \dfrac{t_1}{2}\beta^1_z\right],
\end{cases}
$$

$$\begin{cases} \dfrac{\partial M_\theta^2}{\partial z} = \dfrac{D_{21}^2}{D_{11}^2}\left[Q_z^2 - \dfrac{t_2+t_a}{2}\dfrac{\left(\bar{r}_2 - \dfrac{t_2+t_a}{2}\right)}{\bar{r}_2}\dfrac{G_a}{t_a}\left[u_{z0}^2 + \dfrac{t_2}{2}\beta_z^2 - u_{z0}^1 + \dfrac{t_1}{2}\beta_z^1\right]\right], \\ \dfrac{\partial M_{z\theta}^2}{\partial z} = 0. \end{cases} \tag{A.1}$$

Manuscript received by Editorial Board, November 23, 2017;
final version, July 27, 2018.

## References

[1] N.A. De Bruyne, and R. Houwink (eds). Adhesion and adhesives. Elsevier, 1951.

[2] J.L. Lubkin and E. Reissner. Stress Distribution and Design Data for Tubes. *Journal of Applied Mechanics, Translation ASME*, 78:1213–1221, 1956.

[3] O. Volkersen. Research on the theory of bonded assemblies. *La Construction Métallique*, 4:3–13, 1965. (in French).

[4] R.D. Adams and N.A. Peppiatt. Stress analysis of adhesive bonded tubular lap joint. *Journal of Adhesion*, 9(1):1–18, 1977. doi: 10.1080/00218467708075095.

[5] D. Chen and S. Cheng. Torsional stress in tubular lap joints. *International Journal of Solids Structures*, 29(7)7:845–853, 1992. doi: 10.1016/0020-7683(92)90020-T.

[6] S.R. Graves and D.F. Adams. Analysis of a bonded joint in a composite tube subjected to torsion. *Journal of Composite Materials*, 15(3):211–224, 1981. doi: 10.1177/002199838101500302.

[7] C. Yang. Design and analysis of composite pipe joints under tensile loading. *Journal of Composite Materials*, 34(4):332–349, 2000. doi: 10.1177/002199830003400404.

[8] C. Yang, H. Huang, and Z. Guan. Stress model of composite pipe joints under bending. *Journal of Composite Materials*, 36(11):1331–1348, 2002. doi: 10.1177/0021998302036011167.

[9] J.M. Lees. Behaviour of GFRP adhesive pipe joints subjected to pressure and axial loadings. *Composites Part A: Applied Science and Manufacturing*, 37(8):1171–1179, 2006. doi: 10.1016/j.compositesa.2005.05.033.

[10] J. Hoon Oh. Torque capacity of tubular adhesive joints with different composite adherends. *Materials Letters*, 62(8–9):1234–1237, 2008. doi: 10.1016/j.matlet.2007.08.018.

[11] E. Dragoni and L. Goglio. Adhesive stresses in axially-loaded tubular bonded joints – Part I: Critical review and finite element assessment of published models. *International Journal of Adhesion and Adhesives*, 47:35–45, 2013. doi: 10.1016/j.ijadhadh.2013.09.009.

[12] L. Goglio and D.S. Paolino. Adhesive stresses in axially-loaded tubular bonded joints – Part II: Development of an explicit closed-form solution for the Lubkin and Reissner model. *International Journal of Adhesion and Adhesives*, 48:35–42, 2014. doi: 10.1016/j.ijadhadh.2013.09.010.

[13] A.K. Kaw. *Mechanics of Composite Materials*. 2nd edition. Taylor & Francis Group, LLC., 2006.